Chinese Chemical Letters 36 (2025) 109771

Contents lists available at ScienceDirect

Chinese Chemical Letters

journal homepage: www.elsevier.com/locate/cclet

Mechanism of Fenton catalytic degradation of Rhodamine B induced by microwave and Fe_3O_4

Qinwen Zheng, Xin Liu*, Lintao Tian, Yi Zhou, Libing Liao, Guocheng Lv*

Engineering Research Center of Ministry of Education for Geological Carbon Storage and Low Carbon Utilization of Resources, Beijing Key Laboratory of Materials Utilization of Nonmetallic Minerals and Solid Wastes, National Laboratory of Mineral Materials, School of Material Sciences and Technology, China University of Geosciences, Beijing 100083, China

ARTICLE INFO

Article history:
Received 6 January 2024
Revised 16 February 2024
Accepted 14 March 2024
Available online 16 March 2024

Keywords:
Fe_3O_4
Microwave assisted
Fenton
Rhodamine B
Crystal modification
Catalyze

ABSTRACT

The Fenton method is an effective technology for the removal of organic materials from wastewater. In this work, an induced catalyst Fe_3O_4 was synthesized by a hydrothermal method, and the modulation of the chemical composition of Fe_3O_4 crystals was achieved under the microwave shock method with the same effect as that of calcination treatment. Fe_3O_4 catalyst for the removal of the dye Rhodamine B (RhB) from polluted wastewater under microwave (MW), H_2O_2 system. The results showed that Fe_3O_4 nanomicrospheres prepared by microwave shock exhibited superior catalytic activity under the conditions of 500 W, 0.4 mol/L H_2O_2 and10 mg/L RhB, and the removal rate of RhB reached 98.5% after 10 min. The Fe_3O_4 catalysts also exhibited good stability and degradation efficiency. Electron paramagnetic resonance experiments confirmed that $^{\cdot}OH$ plays a major role in the rapid degradation of RhB. Under microwave action, the catalyst produces electron-hole pairs, in which the holes react with OH^- produced by water ionisation to form $^{\cdot}OH$, and the microwave-treated Fe_3O_4 produces more active species. Fe^{3+} and Fe^{2+} serve as microwave catalytic activity centers and Fenton catalytic activity centers, respectively. This research demonstrates that optimizing the Fe^{2+}/Fe^{3+} ratio significantly enhances the degradation efficiency of RhB. This study presents novel views regarding the mechanism of microwave synergistic catalyst-induced Fenton.

The expansion of dye kinds is occurring progressively due to the rapid advancement of printing and dyeing technology [1,2]. The industrial manufacturing of dyes involves various complex processes, including sulphuration, nitrification, diazotization, reduction, oxidation, and others. Consequently, a substantial volume of wastewater is generated during these processes. The disposal of dyes wastewater has emerged as a critical environmental concern [3–5]. The effluent from dyeing processes exhibits a multifaceted composition, characterized by a high mass concentration of chemical oxygen demand (COD), elevated levels of organic pollutants, intense coloration, and significant toxicity. These properties provide a severe risk of causing carcinogenic, teratogenic, and mutagenic effects [6,7]. Recent studies have indicated that Rhodamine B (RhB) exerts a significant adverse influence on the environment. Hence, it is imperative to employ efficacious approaches to curb the negative effects of contaminants of RhB [8–11].

Previous research has demonstrated the extensive utilization of physical, chemical, and biological techniques, such as adsorption, ion exchange, and biodegradation, with the purpose of eliminating RhB [12]. Nevertheless, the dyes in question possess chemically stable aromatic molecules and a substantial quantity of color-inducing groups, characterized by numerous rings and extended carbon chains. However, conventional methods such as adsorption, electrolysis, biodegradation, and chemical oxidation are inadequate for their efficient removal [13]. In recent years, researchers have shown a growing preference for advanced oxidation technology due to its rapidity, high efficiency, and lack of secondary pollution. This technology is considered efficient and environmentally friendly, and has found widespread application in various production fields, including environmental protection, chemistry, and materials [14–17]. Fenton catalytic oxidation is classified as an advanced oxidation technology that relies primarily on the catalytic decomposition of H_2O_2 by Fe^{2+} to generate a substantial quantity of hydroxyl radicals ($^{\cdot}OH$). With an oxidation electrode potential of 2.80 V, Fenton catalytic oxidation exhibits remarkable oxidation capabilities, surpassed only by fluorine. Consequently, it effectively breaks down numerous organic pollutants into smaller molecules such as H_2O, carbon dioxide, and inorganic salts [18–20]. So, it is essential to note that the conventional Fenton method exhibits

* Corresponding authors.
E-mail addresses: xliu@cugb.edu.cn (X. Liu), guochenglv@cugb.edu.cn (G. Lv).

https://doi.org/10.1016/j.cclet.2024.109771
1001-8417/

a significant reliance on the pH level of the solution [21]. But, a growing number of scholars have shifted their focus towards employing inhomogeneous Fenton system as opposed to the conventional homogeneous Fenton catalysts [22–24]. Aiming to expand the pH response range of the reaction system. The traditional homogeneous Fenton technology has some problems, such as narrow pH response range, difficult recovery and separation of catalyst active components, and secondary pollution caused by iron slime. However, non-homogeneous Fenton technology can effectively overcome the above defects and has a good industrial application prospect [25,26]. Regrettably, the breakdown of organic contaminants in inhomogeneous systems is hindered by sluggish reaction rates, prolonged degradation durations, and excessive H_2O_2 dosages [27–30].

Based on prior research, the utilization of microwaves has been found to induce the generation of oxygen vacancies and electron-hole pairs within the catalyst, which can either participate in the degradation in the reaction system as oxidants, or the holes can react to generate more hydroxyl radicals to degrade the organic pollutants [31–34]. Beyond that, microwaves have the capability to create "hot spot" phenomena and non-thermal effects on the catalyst, which can further enhance the degradation of organic pollutants by Fenton [35–37]. The utilization of microwave shock technology has emerged as a rapid, straightforward, and effective approach for synthesizing materials, which can attain the rational regulation of the chemical composition and morphology of crystals, and then achieve the enhancement of material properties through its "structure-effect" relationship [38–41]. The utilization of microwave-induced oxidation technology relies heavily on the presence of microwave absorbing materials. Fe_3O_4 is a significant transition metal oxide that holds a major role as a microwave-induced oxidizing material [42–44]. This is primarily attributed to the uniqueness of its outer d-electrons and the fact that the degrees of freedom of charge, spin, orbitals as well as lattice are closely correlated with each other, which gives the transition metal oxides a very rich set of structural and physical properties, in particular excellent microwave absorbing properties [45–47].

In this work, we synthesized three-dimensional spherical Fe_3O_4 catalysts using the hydrothermal method and subsequently modified their crystal structure through the application of microwave shock method. Using the representative pollutant RhB as a target, the process conditions such as microwave power, initial concentration and catalyst dosage were optimized to achieve efficient degradation of RhB. More importantly, the elucidation of the mechanism behind the enhancement of Fenton catalysis by microwave irradiation was conducted in a comprehensive manner. Additionally, a potential pathway for the degradation of RhB through microwave-assisted Fenton catalysis was proposed. This research has the potential to enhance our understanding of the mechanism underlying the synergistic effect of it. Furthermore, it offers a new thinking for the removal of dyes from water through synergistic catalytic processes.

Fe_3O_4 microspheres were synthesized through the hydrothermal method using a solution containing 4 mmol of ferric chloride hexahydrate ($FeCl_3{\cdot}6H_2O$) and 0.7 mmol of trisodium citrate dihydrate ($Na_3C_6H_5O_7{\cdot}2H_2O$) in 40 mL of ethylene glycol and stirring for 30 min, followed by the addition of 15 mmol of sodium acetate (CH_3COONa) for 30 min. The above mixed solution was transferred to a stainless-steel autoclave containing 100 mL of polytetrafluoroethylene liner and heated at 200 °C for 10 h. The resulting black precipitate was washed several times with ethanol and deionized water by centrifugation and then dried in an oven at 60 °C for 12 h. The dried sample was named Fe_3O_4-Pristine for the prepared sample.

The modulation of the chemical composition of Fe_3O_4 crystals was mainly achieved by the microwave impact method. A quartz crucible was utilized to contain 500 mg of the prepared Fe_3O_4-Pristine. The crucible is subsequently introduced into a quartz glass container, accompanied by a layer of quartz sand positioned at the base, within a controlled environment glove box that is filled with an argon atmosphere. The uppermost part of the balloon was sealed. Subsequently, the aforementioned apparatus was reacted in a microwave oven at 800 W for 20 s. The designated sample was denoted as Fe_3O_4-Microwave.

To more accurately assess the benefits of the microwave impact method, the Fe_3O_4-Pristine underwent calcination heat treatment for comparative analysis. The Fe_3O_4-Pristine prepared above was placed in a tube furnace under argon atmosphere at 500 °C for 4 h with a temperature increase rate of 5 °C/min, and the sample that underwent the calcination process was designated as Fe_3O_4-Calcination.

Microwave assisted Fenton catalysed degradation experiments: The factors affecting the catalytic degradation of Rhb by Fe_3O_4 under MW conditions were investigated by controlling various variables such as catalyst dosage, Rhb solution concentration, H_2O_2 dosage, MW power and cycle life. A 150 mL Erlenmeyer flask was used as the reaction vessel and a certain amount of Fe_3O_4 and 50 mL of Rhb solution were added to the Erlenmeyer flask each time. The conical flask containing the mixed solution was placed in a laboratory microwave oven and reacted at a specified power for a total of 30 min. Every 5 min during the reaction, 4 mL of the solution was removed from the Erlenmeyer flask and placed in a 7 mL centrifuge tube. The solution in the centrifuge tube was centrifuged at 10,000 rpm for 5 min, after which the concentration of the supernatant was determined and calculated.

To investigate the effect of catalyst dosage on the experiments, five conical flasks containing 10 mg/L Rhb and 0.4 mol/L H_2O_2 solutions with 0.2, 0.4, 1 and 2 g/L Fe_3O_4 were added at 500 W, respectively. To investigate the effect of H_2O_2 dosage on the experiments, five conical flasks containing 10 mg/L Rhb and 1 g/L Fe_3O_4 solutions with 0.1, 0.2, 0.4, 0.6 and 0.8 mol/L H_2O_2 were respectively added at 500 W. To study the effect of Rhb solution concentration on degradation, each conical flask contained 1 g/L Fe_3O_4 and 0.4 mol/L H_2O_2, the MW power was 500 W, and the Rhb concentration was set to 5, 10, 20, and 40 mg/L, respectively. The effect of MW power on the experiments was investigated with 10 mg/L Rhb solution, 1 g/L Fe_3O_4 catalyst and 0.4 mol/L H_2O_2 in each conical flask, and the MW power was set to 200 W, 500 W and 800 W, respectively. To test the lifetime of the catalyst, the reaction power was 500 W and the Erlenmeyer flask contained 10 mg/L Rhb solution, 1 g/L Fe_3O_4 and 0.4 mol/L H_2O_2.

Simultaneously, this study additionally investigated the impact of catalysts in various reaction systems on the degradation of RhB. The catalyst Fe_3O_4 microwave alone, H_2O_2 alone and H_2O_2-Fe_3O_4 microwave systems were selected for the catalytic degradation of RhB in the absence of microwave irradiation. When microwave irradiation was introduced, MW irradiation alone, MW-Fe_3O_4 microwave system, MW-H_2O_2 system and MW-H_2O_2-Fe_3O_4 microwave system were selected for the catalysis of Rhb.

Furthermore, an investigation was conducted to examine the impact of active species produced by the catalysts on the degradation of Rhb. The main active species were first verified by quenching experiments, and IPA, BQ, silver nitrate and EDTA-2Na were chosen as radical bases for scavenging hydroxyl radicals ($\cdot OH$), superoxide radicals (O^{2-}), electrons (e^-) and holes (h^+), respectively, and DMPO as a trap for $\cdot OH$ and O^{2-}, and TEMPO as a trap for h^+ and e^-, respectively.

Fe_3O_4-Microwave was synthesized by the hydrothermal method. The crystal structure composition of the microspheres was modified using the microwave impact method and calcination heat treatment, and the findings are displayed in Fig. 1. The X-ray diffractograms of all the samples displayed characteristic peaks

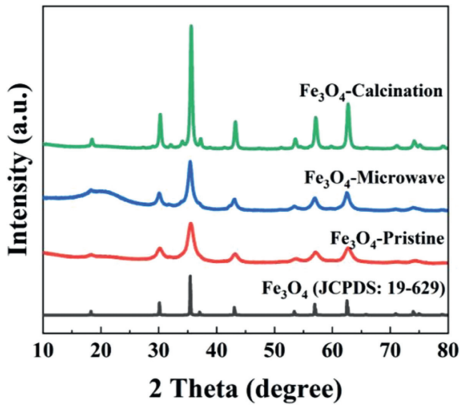

Fig. 1. XRD patterns of Fe_3O_4 prepared by different methods.

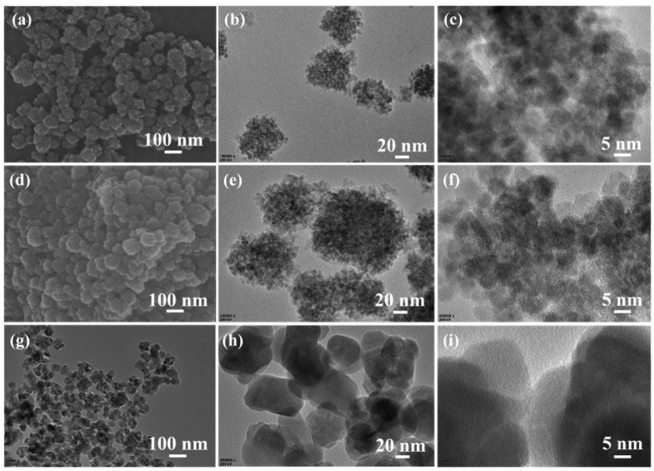

Fig. 2. (a, d, g) Scanning electron microscope images and (b, c, e, f, h, i) transmission electron microscope images of three Fe_3O_4 before degradation reaction.

that matched to the characteristic peaks of the standard card Fe_3O_4 (JCPDS No. 19–629) at specific relative positions. These positions included 18° (111), 30° (220), 35.4° (311), 37° (222), 43° (400), 53.4° (422), 56.9° (511), and 62.5° (440). Additionally, other relative positions of the characteristic peaks were also found to be a match. No substantial variations in peak position were detected, except for the relative intensities of these peaks.

Rietveld refinement is a method that can be employed to ascertain the crystal chemical composition in Fe_3O_4 and get crystal structure data of the sample. The Fe_3O_4 (ICSD: 28664) served as the initial model for Rietveld refinement, and the degraded Fe_3O_4 was then subjected to structure refinement using the TOPAS 4.2 software. The outcomes of this process are presented in Fig. S1 (Supporting information). Where the orange point represents the original diffraction peak intensity, the red line represents the fitted intensity, the blue line represents the difference between the original and fitted intensities, and the green vertical line represents the Bragg position where the diffraction peaks are located for the samples. Fig. S1a displays the Rietveld refinement profile of Fe_3O_4-Pristine, along with the fitting results of the structural refinement in Table S1 (Supporting information), in which the values of R_{wp}, R_{exp}, and R_p are found to get 3.315, 1.847, and 2.500, respectively. These results confirm the reliability of the structural refinement and indicate that the hydrothermally prepared Fe_3O_4 retains its cubic space group. In the crystal structure of Fe_3O_4 which has an antispinel structure, half of the Fe^{3+} are theoretically occupied in tetrahedral coordination (Fe^{3+}-tet.), another half of the Fe^{3+} are occupied in octahedral coordination (Fe^{3+}–oct.), and all of the Fe^{2+} are occupied in octahedral coordination. The occupancies of Fe^{3+}-tet., Fe^{3+}–oct. and Fe^{2+} obtained after Fe_3O_4-Pristine fitting were 0.8511, 0.4090, 0.4090, respectively, and the corresponding ratio of Fe^{2+}/Fe^{3+} was 0.4901and the degraded Fe_3O_4 was then subjected to structure refinement using the TOPAS 4.2 software.

These results confirm the reliability of the structural refinement and indicate that the hydrothermally prepared Fe_3O_4 retains its cubic space group. In the crystal structure of Fe_3O_4, which has an antispinel structure, half of the Fe^{3+} are theoretically occupied in tetrahedral coordination (Fe^{3+}-tet.), another half of the Fe^{3+} are occupied in octahedral coordination (Fe^{3+}–oct.), and all of the Fe^{2+} are occupied in octahedral coordination. The occupancies of Fe^{3+}-tet., Fe^{3+}–oct. and Fe^{2+} obtained after Fe_3O_4-Pristine fitting were 0.8511, 0.4090, 0.4090, respectively, and the corresponding ratio of Fe^{2+}/Fe^{3+} was 0.4901.

The Rietveld refinement figures of Fe_3O_4-Microwave and Fe_3O_4-Calcination are displayed in Figs. S1b and c, respectively, and the fitting results are listed in Table S1, from which it can be seen that the modulation of the chemical composition of the crystals has a negligible effect on the space group, whereas the occupancy of Fe^{3+}-tet. gradually decreases from 0.8511 to 0.8323 (0.8084), the occupancy of Fe^{2+} increased from 0.4090 to 0.4273 (0.4191), and the corresponding ratio of Fe^{2+}/Fe^{3+} increased from 0.4901 to 0.5066 (0.5090). Hence, the microwave shock method may efficiently and rapidly modify the crystal chemical composition of Fe_3O_4, comparable to the effects of calcination heat treatment. The Rietveld refinement profile in Fig. S1d exhibits refinement factors of $R_p = 4.169$, $R_{wp} = 5.482$, and $R_{exp} = 2.099$ after the Fe_3O_4-Microwave degradation process. These values provide evidence of the reliability of the refinement results. The Rietveld refinement analysis confirms that the Fe_3O_4-Microwave, after undergoing the degradation reaction, still maintains its cubic crystal structure with the space group *Fd*-3 m, and the lattice parameter $a = 8.3968$ Å, indicating that there is no alteration in the physical phase compared to before the degradation reaction.

The SEM analysis results of the hydrothermally synthesized Fe_3O_4-Pristine are shown in Fig. 2, from which it can be found that the Fe_3O_4-Pristine morphology presents a microsphere structural morphology with a diameter of about 100 nm (Fig. 2a). The examination of higher magnification TEM images of spherical Fe_3O_4-Pristine demonstrated that the microspheres were formed through the self-assembly of nanoparticles measuring 8–10 nm in size (Figs. 2b and c), which were well facilitated by the use of sodium citrate dihydrate and sodium acetate, respectively, as surfactants and precipitants. Following the application of microwave shock treatment, the morphology of Fe_3O_4-Microwave microspheres exhibited little alterations (Fig. 2d), and the size of the microspheres remained around 100 nm and comprised nanoparticles measuring 8–10 nm.

In contrast, the microsphere morphology of the calcined heat-treated Fe_3O_4-Calcination did not change much after being heated, and their size remained approximately 100 nm, but the size of the constituent nanoparticles gradually changed from 8-10 nm to 20–30 nm. This change could be due to the particles melting during the heating process and the growth of new particles, resulting in the gradual enlargement of the crystalline particles.

The N_2 adsorption-desorption test method was used to study the specific surface area and pore size distribution characteristics of Fe_3O_4 prepared under different conditions, and the results are shown in Fig. 3. The N_2 adsorption-desorption isotherms show that Fe_3O_4 prepared under different conditions has an H3 hysteresis loop at relative pressures of $P/P_0 = 0.8$–1.0 (Fig. 3a), which is typical of Type IV adsorption behaviour [48], suggesting the presence of mesopores formed by the interparticle spacing between the nanoparticles. Furthermore, the BET specific surface areas of

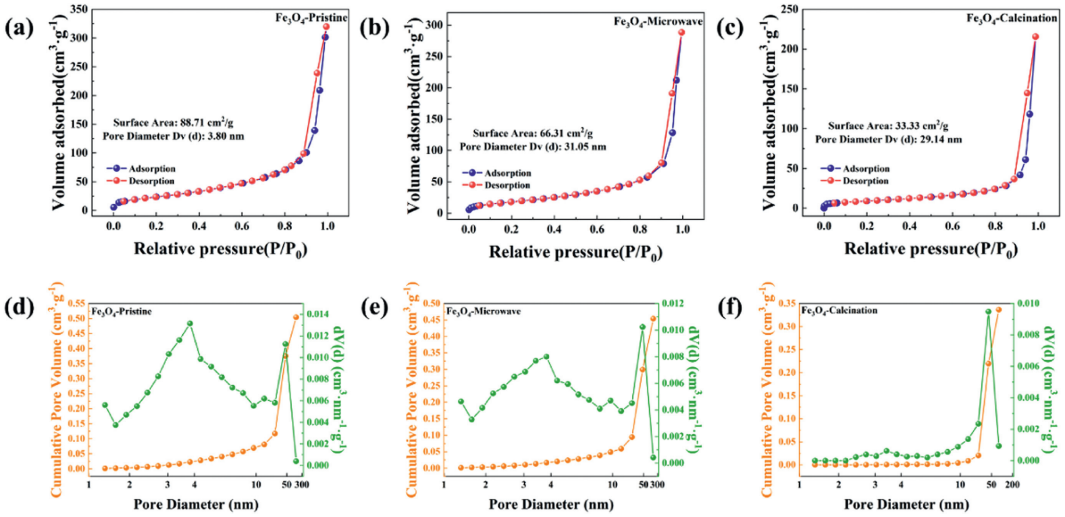

Fig. 3. N_2 adsorption-desorption curves of Fe_3O_4 prepared under different conditions: (a) Fe_3O_4-Pristine, (b) Fe_3O_4-Microwave, (c) Fe_3O_4-Calcination. Corresponding pore size distribution curves of Fe_3O_4 prepared under different conditions: (d) Fe_3O_4-Pristine, (e) Fe_3O_4-Microwave, (f) Fe_3O_4-Calcination.

Fe_3O_4-Pristine, Fe_3O_4-Microwave, and Fe_3O_4-Calcination were calculated to be up to 88.71, 66.31, and 33.33 m^2/g, respectively. The pore size distribution curves of Fe_3O_4-Pristine, Fe_3O_4-Microwave and Fe_3O_4-Calcination were obtained according to the Barrette-Joynere-Halenda (BJH) method to obtain the pore size distribution curves are shown in Figs. 3d-f, most of the size distribution of Fe_3O_4-Pristine is between 2 nm and 10 nm, with an average pore size of 3.80 nm, and most of the pore size distribution of Fe_3O_4-Microwave is around 30 nm, with an average pore size of 31.05 nm, and most of the pore size distribution of Fe_3O_4-Calcination is also around 30 nm, with an average pore size of 29.14 nm. The Fe_3O_4 microspheres exhibit a mesoporous structure that is advantageous for catalytic degradation. This is due to the increased number of active sites resulting from the larger specific surface area. Additionally, the mesoporous structure acts as a channel for efficient mass transfer, facilitating the swift transportation of reactants and products during the catalytic reaction. Still, the specific surface area of the catalysts decreased during microwave impingement or calcination heat treatment, and the effect of specific surface area on the results of the subsequent experiments can be excluded based on the difference in the subsequent degradation performance of RhB.

X-ray photoelectron spectroscopy was used to further examine the chemical composition and electronic structure of Fe_3O_4 produced under various conditions. The findings are presented in Fig. 4. The Fe 2p energy level spectra of Fe_3O_4-Pristine may be acquired from Fig. 4a, revealing two prominent peaks located at approximately 724.5 eV and 710.5 eV, which correspond to the Fe $2p_{1/2}$ and Fe $2p_{3/2}$ spin-orbit components of the Fe 2p peak of Fe_3O_4, accordingly. The Fe 2p peak can be resolved into individual peaks corresponding to Fe^{3+}, Fe^{2+}, and satellite peaks. The binding energies of 710.39 eV and 723.54 eV are associated with Fe^{3+}, while the binding energies of 713.13 eV and 726.25 eV are associated with Fe^{2+}. Also, the peaks seen at energy levels of approximately 716.33 and 729.48 eV correspond to vibrational satellites of Fe^{3+}, while the peaks at 719.36 and 733.14 eV correspond to vibrational satellites of Fe^{2+}. The presence of both Fe^{2+} and Fe^{3+} indicates the production of Fe_3O_4, which aligns with the findings of the XRD study [49,50].

The results of Fe 2p fitting for Fe_3O_4-Microwave and Fe_3O_4-Calcination are shown in Figs. 4c and e, respectively, and the content and ratio of Fe^{3+} and Fe^{2+} in the corresponding crystal structures are shown in Table S2 (Supporting information). From the table, it can be found that compared with Fe_3O_4-Pristine, the ratio

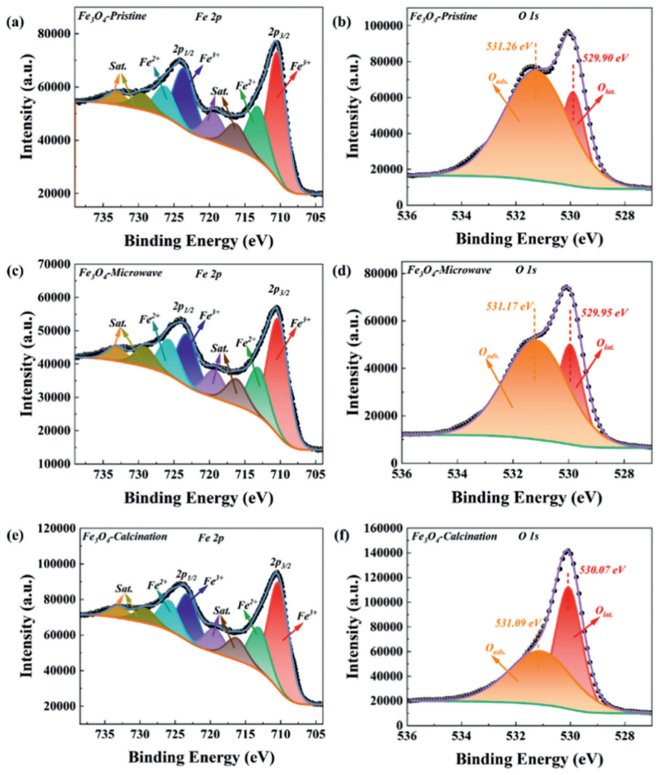

Fig. 4. XPS patterns of Fe_3O_4 prepared under different conditions: (a) Fe 2p and (b) O 1s for Fe_3O_4-Pristine. (c) Fe 2p and (d) O 1s for Fe_3O_4-Microwave. (e) Fe 2p and (f) O 1s for Fe_3O_4-Calcination.

of Fe^{2+}/Fe^{3+} in Fe_3O_4-Microwave increased from 0.4817 to 0.4980, which, firstly, indicates that the microwave treatment under argon atmosphere can modulate the crystal structure composition of Fe_3O_4. And secondly, it demonstrates that microwave treatment can achieve a crystal chemical composition similar to that of the calcination treatment, confirming the microwave's ability to naturally and efficiently modulate the crystal structure. This provides additional evidence that microwaves are uncomplicated and effective in controlling the crystal structure of Fe_3O_4. In addition, as shown in Fig. 4b, the peak of O 1s is fitted into two sub-peaks,

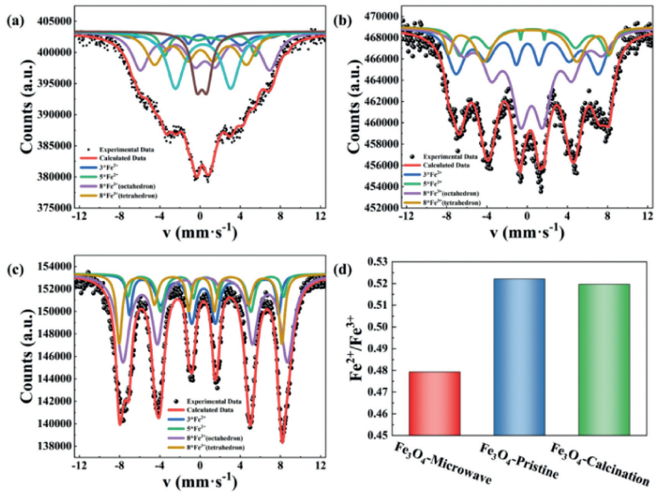

Fig. 5. ^{57}Fe Mössbauer spectra of Fe_3O_4 prepared under different conditions: (a) Fe_3O_4-Pristine, (b) Fe_3O_4-Microwave, (c) Fe_3O_4-Calcination, and (d) the Fe^{2+}/Fe^{3+} ratio obtained from the fitting.

$O_{ads.}$ is a water molecule or hydroxyl group adsorbed on the surface, which corresponds to a binding energy of 531.26 eV. $O_{lat.}$ is a characteristic peak of Fe_3O_4 lattice oxygen, with a corresponding binding energy of 529.90 eV, and further presents more evidence for the presence of Fe_3O_4.

In conjunction with the fitting outcomes, it becomes evident that hydrothermal heating increases the amount of adsorbed oxygen in Fe_3O_4. This can be ascribed to the presence of residual organic matter in the raw materials (trisodium citrate dihydrate and sodium acetate) or to the organic molecules that bonded during the reaction, as further corroborated by the diffraction peaks in the XRD pattern.

Mössbauer spectroscopy is widely employed in the investigation and determination of the chemical state of Fe. This is primarily attributed to the correlation that exists between the chemical state of the compound and one of the Mössbauer parameters, the homogeneous isoenergetic shift [51,52]. The Mössbauer spectrum can be analysed to extract specific parameters, such as the isomass energy shift (I.S.), quadrupole splitting (Q.S.), linewidth (Γ), and the area of resonance absorption (Area). This analysis provides information about the electrons and structure of the iron in the sample [53]. The ^{57}Fe Mössbauer spectra of Fe_3O_4 prepared under different conditions are shown in Fig. 5.

In contrast to the six-line spectrum documented in the literature [54], the six-line spectrum of Fe_3O_4-Pristine exhibits a notable broadening and the emergence of a series of double peaks (Fig. 5a). In Mössbauer spectroscopy, Magnetic single-domain particles exhibit a critical size for superparamagnetism. When the particle size is smaller than this critical size, the particles become magnetically disordered and superparamagnetic, resulting in a Mössbauer spectrum with either a single peak or double peaks. On the other hand, when the particle size exceeds the critical size, the particles become magnetically ordered and exhibit either ferromagnetism or ferrimagnetism. This corresponds to the Mössbauer spectrum showing the splitting of the six-line spectrum. Combining SEM results, it is evident that the Fe_3O_4 particles synthesized in this study possess a single domain structure, since their critical size is approximately 128 nm. After microwave treatment, the size of the Fe_3O_4-Microwave particles undergoes an increase, resulting in the splitting of the Mössbauer spectral lines into six-line spectrum. Especially after heat treatment, the crystallinity of Fe_3O_4-Calcination is notably improved, and the particle size increases significantly. The Mössbauer spectral lines exhibit a clearly divided six-line spectrum, consisting of two sets of magnetically split six-line spectrum.

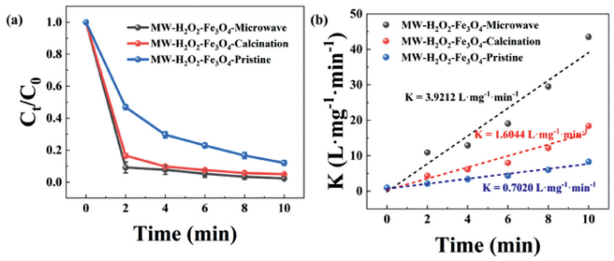

Fig. 6. (a) Effect and (b) degradation rate of Fe_3O_4 with different crystal chemical components prepared under different conditions on microwave-assisted Fenton catalytic degradation of RhB.

Additionally, the determination of Fe ion occupation in tetrahedral and octahedral cavities within Fe_3O_4 crystals was carried out through the analysis of spectral lines associated with the A and B sites. When the Fe_3O_4-Pristine is examined in conjunction with the ^{57}Fe Mössbauer spectral fitting parameters listed in Table S3 (Supporting information), it primarily consists of four sets of spectral fits: 8^*Fe^{3+} (tetrahedron), 8^*Fe^{3+} (octahedron), 5^*Fe^{2+}, and 3^*Fe^{2+}. The respective contents of these sets are approximately 74.3%, 2.2%, 2.0%, and 17.21%, respectively. Thus, the Fe^{2+}/Fe^{3+} ratio is calculated to be 0.4792. The Fe^{2+}/Fe^{3+} ratios in Fe_3O_4 after microwave and calcined heat treatments were 0.5220 and 0.5197, respectively. These values closely matched the results obtained from Rietveld refinement and XPS analysis, providing further evidence that microwave treatment can achieve the same effect as high-temperature heat treatment.

Fe_3O_4 with varying crystal chemical compositions, prepared under varied conditions, is anticipated to serve as catalysts to enhance the degradation of contaminants through microwave-assisted Fenton-catalysis. Fig. 6a illustrates the impact of Fe_3O_4 catalysts with varying crystal chemical compositions, prepared under different conditions, on the microwave-assisted Fenton-catalysed degradation of RhB. It is clear that the Fe_3O_4-Microwave catalyst, subjected to microwave treatment, exhibits the highest effectiveness in degrading RhB. Primarily on the previous analyses, it is clear that the Fe^{2+}/Fe^{3+} content of microwave-treated Fe_3O_4-Microwave is the highest. The Fe^{2+}/Fe^{3+} content and degradation effect of heat-treated Fe_3O_4-Calcination is medium, while the degradation effect of Fe_3O_4-Pristine is the poorest. This suggests that the Fe^{2+}/Fe^{3+} content is the crucial factor influencing microwave-assisted catalytic degradation. The catalytic efficiency of Fe_3O_4 was significantly augmented when the concentrations of both Fe^{2+} and Fe^{3+} in the catalyst were suitable. The reaction kinetic constants of Fe_3O_4-Microwave were enhanced by 5.6 and 2.4 times when compared to Fe_3O_4-Pristine and Fe_3O_4-Calcination (Fig. 6b), accordingly. Among the catalysts, Fe_3O_4-Microwave with the highest Fe^{2+}/Fe^{3+} ratio of 2.23 exhibited the most effective co-catalytic activity. Therefore, in the MW-H_2O_2-Fe_3O_4 system, Fe^{3+} acts as the active site for microwave catalysis. Increasing its content promotes the generation of more active species and enhances microwave absorption, thereby maximising the hot spot effect and non-thermal effect of microwaves. Both are necessary for the microwave-assisted Fenton-catalysed degradation of RhB in this system.

Given that MW-H_2O_2-Fe_3O_4-Microwave system exhibits superior degradation performance in microwave-assisted Fenton-catalysed degradation of RhB. To expedite the degradation of RhB, we investigated the elements that affect RhB degradation in the MW-H_2O_2-Fe_3O_4-Microwave system by manipulating variables such as catalyst dosage, H_2O_2 dosage, initial RhB concentration, and microwave power.

The amount of catalyst used has the most direct effect on the degradation of RhB through microwave-assisted Fenton-catalytic

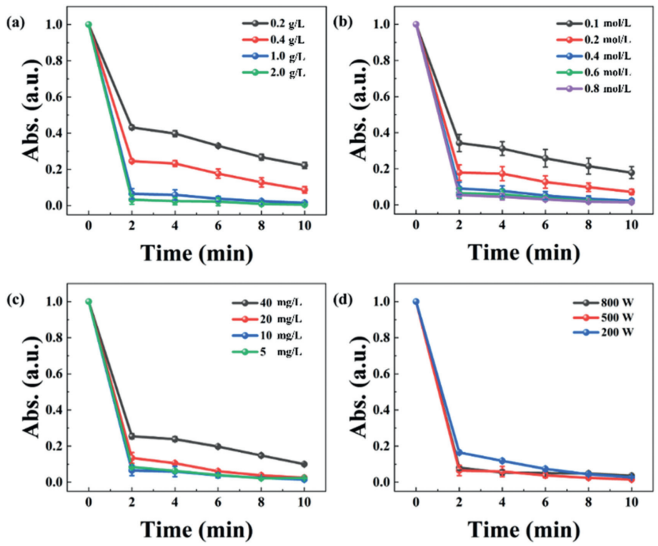

Fig. 7. (a) Effect of catalyst dose, (b) H_2O_2 dose, (c) initial RhB concentration and (d) microwave power on the degradation of RhB by MW-H_2O_2-Fe_3O_4-Microwave system.

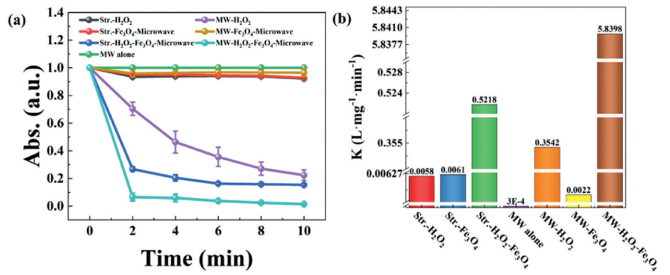

Fig. 8. (a) Degradation of RhB by Fe_3O_4-Microwave in different reaction systems and (b) the corresponding secondary kinetic constants.

process. Hence, this study examined the impact of Fe_3O_4-Microwave dosage on the degradation of RhB by the MW-H_2O_2-Fe_3O_4-Microwave system. The order of RhB removal efficiency, as evident from Fig. 7a, is as follows: Fe_3O_4-Microwave (2.0 g/L) > Fe_3O_4-Microwave (1.0 g/L) > Fe_3O_4-Microwave (0.4 g/L) > Fe_3O_4-Microwave (0.2 g/L), and there is a positive correlation between the catalyst amount and the efficiency of RhB degradation. Increasing the catalyst dosage from 2.0 g/L to 2.0 g/L resulted in an increase in the degradation of RhB from 77.8% to 99.4%. It can be attributed to the direct impact of catalyst dosage on the catalytic active sites, which enhances the Fenton reaction and leads to the generation of more hydroxyl radicals with potent oxidative properties. Consequently, the degradation efficiency of RhB is accelerated. Given the expenses associated with catalyst preparation and the focus on environmentally friendly practises, a dose of 1.0 g/L of Fe_3O_4-Microwave catalysts was chosen for a series of subsequent experimental investigations.

The dose of H_2O_2 is a crucial component that influences the degrading effect of RhB in the direct MW-H_2O_2-Fe_3O_4-Microwave system. The impact of various amounts of H_2O_2 on the elimination of RhB may be shown in Fig. 7b. The data presented in clearly demonstrate that the order of RhB removal efficiency is as follows: H_2O_2 (0.8 mol/L) > H_2O_2 (0.6 mol/L) > H_2O_2 (0.4 mol/L) > H_2O_2 (0.2 mol/L) > H_2O_2 (0.1 mol/L), and it is evident that the dosage of H_2O_2 is directly proportional to the degradation efficiency of RhB. The increase in H_2O_2 content from 0.1 mol/L to 0.8 mol/L reflected in an increase in the degrading effect of RhB from 82.1% to 98.5%. The absence of H_2O_2 also results in the absence of potent oxidising hydroxyl radicals generated by Fenton activation. This phenomenon exhibits a strong resemblance to the findings of prior investigations [55–57]. In comparison to the conventional Fenton reaction, this system demonstrates the capability to efficiently degrade RhB while necessitating significantly less H_2O_2. Considering the expenses associated with subsequent experimental studies, an H_2O_2 concentration of 0.4 mol/L was chosen.

The results of microwave-induced RhB degradation at different RhB initial concentrations are shown in Fig. 7c. The Fe_3O_4-Microwave exhibited degradation efficiencies of 90%, 97.5%, 98.5%, and 99.9% for RhB at starting concentrations of 5, 10, 20, and 40 mg/L, respectively. Moreover, it was discovered that the augmentation in the initial concentration of RhB not only had a more notable impact on the efficiency of degradation, but also on the pace of degradation. The primary reason for this is the low concentration of catalyst in the system. As the concentration of RhB pollutant increases, a significant number of RhB molecules attach to the catalyst's surface and incompletely degraded intermediates hinder further degradation, thus leading to a decrease in the degradation efficiency and degradation rate of RhB. The initial concentration of RhB was chosen to be 10 mg/L in a series of subsequent experimental studies.

The degrading efficiency of RhB in the MW-H_2O_2-Fe_3O_4-Microwave system (Fig. 7d) was significantly influenced by the microwave power. The degrading reaction of 50 mL of RhB with a concentration of 10 mg/L under microwave irradiation primarily took place within the initial 2 min. By increasing the microwave power from 200 W to 800 W, the degrading efficiency of TC improved from 96.4% to 97.3% within the initial 2 min period. The degradation efficiency and removal rate exhibited a substantial increase within a brief duration, whereas the degradation efficiency and microwave power demonstrated a simultaneous increase. At a reaction time of 10 min, the degradation efficiencies were essentially equal across the power range of 200–800 W. So, augmenting the microwave power can significantly reduce the reaction time and enhance the degrading efficiency. This is because the increase of microwave power, on the one hand, enhances the microwave catalytic activity of Fe_3O_4-Microwave to a certain extent, and its "hot spot" and non-thermal effects can promote the degradation of RhB. On the other hand, the microwave effectively facilitates the generation of more powerful oxidative hydroxyl radicals in the Fenton system. The combined effect of these two factors significantly enhances the efficiency of RhB degradation. The subsequent series of experiments were selected as the microwave power of 500 W.

The role of the synergistic reaction in RhB degradation was confirmed through catalytic tests conducted in several reaction systems. The degradation of RhB under different experimental circumstances is illustrated in Fig. 8. The figure demonstrates that lacking microwave irradiation, the catalyst Fe_3O_4-Microwave alone (Str.-Fe_3O_4-Microwave) and H_2O_2 alone (Str.-H_2O_2) only managed to degrade RhB by 7.8% and 7.4% respectively, and RhB degradation was minimal in these cases. The degradation efficiency of RhB in the H_2O_2-Fe_3O_4-Microwave system was 85.6%. This high efficiency can be attributed to the ability of the transition metal ion Fe^{2+} to generate reactive chemicals (•OH) when combined with hydrogen peroxide, while the catalytic adsorption of RhB had a minor role in the degradation process. The introduction of microwave irradiation resulted in a degradation efficiency of 3.6% for the MW-Fe_3O_4-Microwave system. Observably, the microwave radiation catalyst generates a "hot spot" that leads to a localised rise in temperature on the catalyst surface, but only a portion of the RhB is degraded as a result. The MW-H_2O_2 system exhibited a degradation efficiency of 77.6% for RhB, indicating that microwaves can induce the production of hydroxyl radicals from hydrogen peroxide to fa-

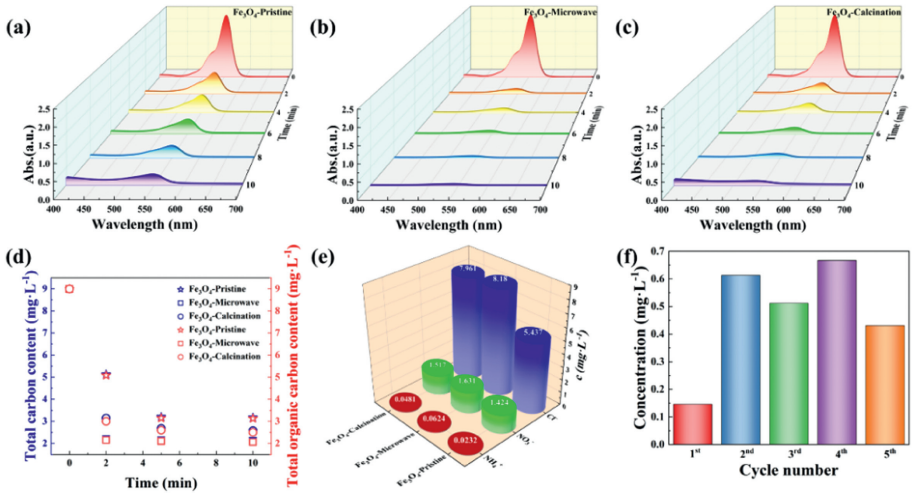

Fig. 9. UV–vis absorption spectra of catalytic degradation of RhB in different reaction systems: (a) Fe_3O_4-Pristine, (b) Fe_3O_4-Microwave, (c) Fe_3O_4-Calcination, (d) TC and TOC in catalytic degradation of RhB in different reaction systems. (e) Ionic concentration, (f) leaching concentration of Fe after catalytic degradation of RhB in the MW-H_2O_2-Fe_3O_4-Microwave system.

cilitate the breakdown of RhB. Thus, the use of microwaves greatly augmented the efficacy of H_2O_2 in eliminating contaminants, and the inclusion of Fe_3O_4-Microwave further intensified the decontamination potential of H_2O_2. The Fe_3O_4-Microwave catalyst exhibited exceptional performance, achieving a degrading efficiency of up to 98.5% for RhB. The kinetic constants for the degradation of RhB in the MW-H_2O_2-Fe_3O_4-Microwave system were found to be 11.2 and 16.5 times greater than those for the Str.-H_2O_2-Fe_3O_4-Microwave and MW-H_2O_2 systems, respectively (Fig. 8b). Hence, the utilisation of catalyst and microwave may efficiently facilitate the degradation of RhB through Fenton reaction, and can further optimise the process by adjusting the crystal chemical composition.

The examination of a catalyst's structure and performance is crucial in determining its reusability, which in turn defines the catalyst's universality in practical wastewater treatment. Hence, we investigated the effectiveness of RhB degradation using Fe_3O_4-Microwave catalysts in the MW-H_2O_2-Fe_3O_4 system during five cycles. Following each experiment, the solution that had undergone a reaction was allowed to settle and then subjected to centrifugation. The resulting catalyst was subsequently dried in an oven and utilised for the subsequent cycle of the experiment (Fig. S2 in Supporting information). The degrading efficiency of RhB showed a progressive decline as the number of cycles of Fe_3O_4-Microwave catalyst increased. Upon initial use, the Fe_3O_4-Microwave catalyst exhibited a degrading efficiency of 98.5% for RhB in solution. Even after undergoing five cycles of use, the Fe_3O_4-Microwave catalyst maintained a high level of catalytic activity. The degradation efficiency of RhB was measured at 95%, providing further evidence of the catalyst's stability and capacity to be reused in the MW-H_2O_2-Fe_3O_4 system.

The mineralization of organic contaminants is crucial for the degradation process of microwave-assisted Fenton catalysis. The degree of mineralisation of organic contaminants was determined using UV–visible spectrophotometry. From Figs. 9a-c, it is evident that the decrease in absorbance of Fe_3O_4-Microwave after the degradation of RhB is more pronounced compared to Fe_3O_4-Pristine and Fe_3O_4-Calcination. This suggests that RhB and its intermediates are gradually breaking down. In contrast, the intensity of the peaks at the corresponding wavelengths is noticeably higher in the other two systems. The results are further supported by the measurements of TOCs and total carbon throughout the entire degradation process. Based on the data presented in Fig. 9d, it is evident that the levels of total carbon and total organic carbon in the three systems experienced a rapid decline at 2 min. Subsequently, there was only a slight variation as time progressed. Yet, in the Fe_3O_4-Microwave system, the levels of total carbon and total organic carbon decreased more significantly over time. This suggests that the system effectively achieved the mineralization of RhB. Furthermore, the two values were closely aligned, indicating that the carbon in the solution was predominantly mineralized in the form of inorganic carbon (CO_2). When thinking about the chemical composition of RhB and the ion chromatography results (Fig. 9e), it is clear that the Fe_3O_4-Microwave system exhibited a greater concentration of Cl^- in the solution following the degradation of RhB, in comparison to the Fe_3O_4-Pristine and Fe_3O_4-Calcination systems. This indicates that the catalyst effectively enhances the Fenton reaction in conjunction with microwave energy. Also, the mineralized nitrogen primarily exists in the form of NO_3^- and NH_4^+. And when comparing the leaching concentration of Fe in the solution after five degradation cycles to the original RhB solution, it was observed that the concentration ranged from 0.146 mg/L to 0.667 mg/L at the first instance (Fig. 9f). This concentration level complies with the wastewater discharge standard. The small amount of Fe detected in the solution may originate from the residue in the centrifuged catalyst, indicating that the degraded solution does not cause any secondary pollution to the environment. Thus, the Fe_3O_4-Microwave catalyst has remarkable structural stability in the degradation environment, making it suitable for the microwave-assisted Fenton process to mineralize RhB.

An investigation of the process by which degradation occurs is beneficial for advancing the research and design of catalysts, as well as for proposing degradation pathways. which in turn, allows for the optimisation of the experimental design for microwave-assisted Fenton-catalysed degradation of RhB. The active species in the MW-H_2O_2-Fe_3O_4 system for the degradation of RhB were identified using EPR tests. The results of the tests, using DMPO as a trapping agent for $^{\bullet}OH$ and $O_2^{\cdot-}$ and TEMPO as a trapping agent for h^+ and e^-, are demonstrated in Fig. S3 (Supporting information). Upon subjecting the solution to microwave radiation for a duration of 10 min, Fig. S3a revealed a quadruple peak intensity ratio of 1:2:2:1 for DMPO-$^{\bullet}OH$, confirming the presence of $^{\bullet}OH$ in the system. Further, the spectrograms for DMPO-$O_2^{\bullet-}$ exhibited a quadruple peak intensity ratio of 1:1:1:1, indicating the presence of $O_2^{\bullet-}$ in the system. Moreover, based on the triple peak intensity

ratio of 1:1:1 found for TEMPO-h^+ and TEMPO-e^- in Figs. S3c and d, respectively, it may be inferred that the system contains both h^+ and e^-. The EPR results revealed that the Fe_3O_4 reaction system, prepared under various conditions, generated different numbers of active species, with the order being $^{\bullet}OH > h^+ > e^- > O_2^{\bullet-}$. The presence of $^{\bullet}OH$ played a significant role in the rapid degradation of RhB. Furthermore, Fe_3O_4-Microwave exhibited a more substantial production of active species (particularly $^{\bullet}OH$) compared to Fe_3O_4-Pristine and Fe_3O_4-Calcination. This learning aligns with previous experimental results, which indicated that a better Fe^{2+}/Fe^{3+} ratio is favourable for the degradation of organic pollutants.

In extra to the outcomes given in Fig. S3, the MW-H_2O_2-Fe_3O_4 system detected a greater plenty of $^{\bullet}OH$ characteristic peaks. The reason for this can be attributed to the phenomenon that, when subjected to microwaves, the catalyst generates electron-hole pairs (Eq. 1). The holes then react with OH^- ions produced through water ionisation, resulting in the formation of OH (Eqs. 2 and 3). Fe_3O_4-Microwave containing Fe^{2+} active site also to generate the active species OH by Fenton reaction (Eq. 4). The microwave can also directly stimulate hydrogen peroxide to produce the active species $^{\bullet}OH$ (Eq. 5), which is the primary factor responsible for the breakdown of RhB in the MW-H_2O_2 system. Beyond that, electrons will undergo a reaction with dissolved O_2 in water, which resulted in the generation of the $O_2^{\cdot-}$ (Eq. 6), and this radical can also participate in the breakdown process of RhB. Thus, while the degradation of RhB through microwave-assisted Fenton catalysis is a multifaceted process that encompasses several reactive species and is influenced by factors such as microwave-induced thermal and non-thermal effects (Eq. 7).

$$Fe_3O_4 + MW \rightarrow Fe_3O_4\ (h^+ + e^-) \quad (1)$$

$$H_2O + MW \rightarrow {}^{\bullet}OH + {\cdot}H \quad (2)$$

$$h^+ + OH^- \rightarrow {}^{\bullet}OH \quad (3)$$

$$Fe_3O_4\ (Fe^{2+}) + H_2O_2 \rightarrow Fe_3O_4\ (Fe^{3+}) + {}^{\bullet}OH + OH^- \quad (4)$$

$$H_2O_2 + MW \rightarrow {}^{\bullet}OH \quad (5)$$

$$e^- + O_2 \rightarrow O_2^{\bullet-} \quad (6)$$

$$\text{Pollutant (RhB)} + {}^{\bullet}OH/\ O_2^{\bullet-}/\ h^+/\ e^- \rightarrow \text{Degradation intermediates} \quad (7)$$

As mentioned above, Fe_3O_4 exhibits a proclivity to undergo an increase in Fe^{2+} following microwave or calcination heat treatment in an argon atmosphere, while Fe^{3+} experiences the converse alteration. The presence of dual catalytic active sites in the catalyst is essential for the process of microwave-assisted Fenton. Hence, an investigation was conducted to determine the specific functions of these active sites in microwave catalysis and Fenton catalysis, and the findings are presented in Fig. 10. Firstly, Fe_3O_4 belongs to a category of materials known as magnetically lossy materials in which the electronic spin magnetic moment is a key factor affecting the magnetic loss, which is closely connected to the unpaired electrons of the ions. Several studies have demonstrated that the electronic spin magnetic moment plays a crucial role in the microwave loss mechanism, which in turn has a substantial impact on the degradation of organic matter catalysed by microwaves. The electronic configuration of Fe^{3+} at the octahedral or tetrahedral position in Fe_3O_4 is $t_{2g}^2e_g^3$ [58]. Similarly, the electronic configuration of Fe^{2+} at the octahedral position is $t_{2g}^2e_g^4$. Thus, the number of unpaired

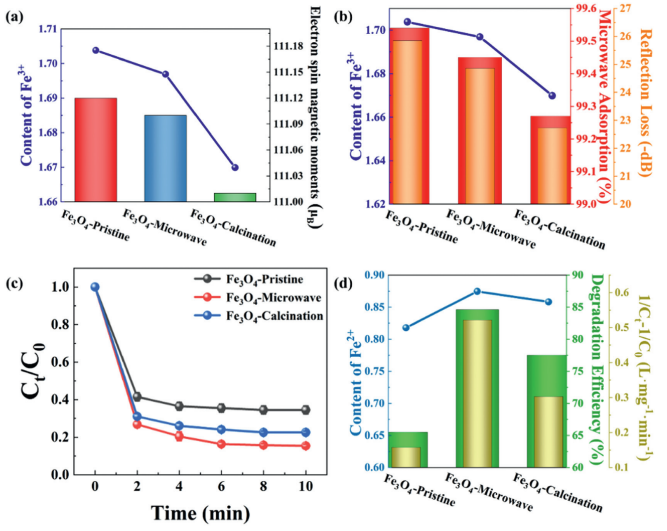

Fig. 10. The content of Fe^{3+} in Fe_3O_4 with different crystal chemical components prepared under different conditions and the corresponding: (a) Electron spin magnetic moments, (b) microwave reflection loss and microwave absorption. (c) Effect of Fe_3O_4 with different crystal chemical components prepared under different conditions on Fenton catalytic degradation of RhB.

electrons in Fe^{3+} and Fe^{2+} is 5 and 4, respectively. These unpaired electrons result in corresponding electronic spin magnetic moments of 5 μB and 4 μB. The Rietveld refinement analysis revealed that the treatment resulted in a reduction in the Fe^{3+} content in the catalyst. Additionally, the unit cell spin magnetic moments for Fe_3O_4-Pristine, Fe_3O_4-Microwave, and Fe_3O_4-Calcination were calculated to be 111.12 μB, 111.10 μB, and 111.01 μB, respectively (Fig. 10a). Thus, the existence of Fe^{3+} as the active site of the catalyst in microwave-assisted Fenton-catalysed degradation of dyes can significantly improve performance by producing "hot spot" and non-thermal effects. In Fig. 10b, the microwave reflectances of Fe_3O_4-Pristine, Fe_3O_4-Microwave, and Fe_3O_4-Calcination were −25.85, −24.86, and 22.73 dB, respectively. Generally speaking, a measurement of −10 dB indicates that the sample's microwave absorption may achieve 90%, while a measurement of −20 dB indicates that the sample's microwave absorption can achieve 99%. Based on the aforementioned findings, it is evident that a decrease in the Fe^{3+} content in the catalyst leads to a gradual decrease in the electronic spin magnetic moment and microwave reflectivity. This observation aligns with the excellent microwave absorption activity of Fe_3O_4-Pristine.

By eliminating the possibility of dyes being adsorbed physically by the samples, Fig. 10c demonstrates the pattern of Fenton-catalysed degradation of RhB by Fe_3O_4, which was prepared under various conditions. The figure reveals that the redox reaction primarily takes place within the initial 2 min, and the degradation of RhB gradually intensifies as the Fe^{3+} content decreases. likewise, the reaction rate constants were computed and compared using pseudo-secondary kinetics, which were applied to the catalytic degradation of RhB by Fe_3O_4 Fenton produced at various conditions. The results revealed a positive relationship between the rate constants and the variation in Fe^{2+} content. Thus, the presence of Fe^{2+} as the catalytic active site in the Fenton redox system, along with its active species generated during the Fenton redox process, can significantly improve the efficiency of dye degradation. Out all the options, the Fe_3O_4-Microwave, which was treated with a microwave, demonstrated the most effective degrading performance. In contrast, the Fe_3O_4-Pristine and Fe_3O_4-Calcination showed unsatisfactory results due to the absence of Fe^{2+} and Fe^{3+} respectively.

Microwave-assisted Fenton-catalysed degradation of RhB is a complex process. To gain a comprehensive comprehension of the intermediates generated during the degradation of RhB, the solutions were subjected to reactions for durations of 2, 5, and 10 min in the Fe_3O_4-Pristine, Fe_3O_4-Microwave, and Fe_3O_4-Calcination degradation systems. Subsequently, the solutions were identified and analysed using liquid chromatography-mass spectrometry (LC-MS). To further analyse the resulting intermediates, the intermediate structures were acquired using mass spectrometry analysis of samples that were eluted in a high liquid state for 0.9 min and 21.9 min, which were evaluated using positive ion mode (EIS+). The degradation of RhB occurred in three different systems: Fe_3O_4-Pristine, Fe_3O_4-Microwave, and Fe_3O_4-Calcination. The degradation process lasted for 2, 5, and 10 min in each system, respectively. The mass spectra corresponding to these degradation processes can be found in Fig. S4 (Supporting information). The precise molecular weight of the product can be determined by analysing the quasi-molecular ion $[M+H]^-$. After 21.9 min of elution, the mass spectra of the initial RhB solution revealed a *quasi*-molecular weight of $m/z = 443.2269$ as the molecular weight of RhB. With an increase in reaction time, RhB underwent steady degradation, resulting in the formation of several intermediates, as indicated by the mass spectra.

The application of liquid phase-mass spectrometry enabled the identification of the intermediates generated by the degradation of RhB using microwave-assisted Fenton catalysis, and to speculate on the RhB degradation mechanism and degradation pathway during the degradation process. A total of eleven intermediates were identified using LC-MS, and the hypothetical degradation pathway of RhB is illustrated in Fig. S5 (Supporting information). It illustrates that the degradation of RhB may be primarily categorised into four distinct steps [59,60]: (1) The process of N-deethylation. The RhB molecule ($m/z = 443.2269$) undergoes progressive assault by hydroxyl radicals, resulting in deethylation and the formation of *N*,*N*–diethyl-*N*-ethylrhodamine (**R1**, $m/z = 414.1937$), as well as aminorhodamine (**R2**, $m/z = 254.9364$), (**R3**, $m/z = 238.9589$), (**R4**, $m/z = 222.9212$). (2) Cleavage of conjugated chromophore. The chromophore of the demethylated intermediate was destroyed and cleaved to the products **R5** ($m/z = 152.9975$), **R6** ($m/z = 150.0278$), **R7** ($m/z = 149.9978$) and **R8** (144.0278). (3) Ring opening. The benzene ring opens into small molecular compounds such as 1,1,4,4-butanetetrol (**R9**, $m/z = 122.0331$) and 4-methylpentanoic acid (**R10**, $m/z = 124.9788$). (4) Mineralisation. Small molecule compounds are eventually further mineralised to CO_2 and H_2O.

In this work, we have synthesised nanosized microspheres of Fe_3O_4 by a hydrothermal approach. This involved modifying the chemical composition of Fe_3O_4 crystals utilising microwave shock and high temperature calcination. An investigation was conducted to examine the impact of catalyst dosage, H_2O_2 dosage, RhB starting concentration, and microwave power on the degradation of RhB. Under the specified experimental settings of Fe_3O_4-Microwave = 1.0 g/L, H_2O_2 = 0.4 mol/L, RhB = 10 mg/L, MW power = 500 W, the findings demonstrated a removal rate of 98.5% for RhB after 10 min of treatment. It shows that the catalyst has excellent degradation performance. After a treatment duration of 10 min, the results indicated that the elimination efficiency of RhB was 98.5%. The cycle life experiments confirmed the exceptional structural stability and reusability of the Fe_3O_4-Microwave catalyst. The tests demonstrate that Fe^{3+} and Fe^{2+} can serve as the microwave catalytic activity centre and Fenton catalytic activity centre, respectively, thereby significantly enhancing the degradation efficiency. Compared with Fe_3O_4-Pristine and Fe_3O_4-Calcination systems, the reaction rate of Fe_3O_4-Microwave system was increased by 5.6 times and 2.4 times, respectively. Analysis of the degradation mechanism showed that hydroxyl radicals ($^{\bullet}OH$) play an important role as the main active species in the whole degradation of the system. Microwave synergistic Fe_3O_4-Microwave-assisted Fenton degradation of RhB was more complete and could lead to the mineralisation of RhB.

Declaration of competing interest

The authors declare that they have no known competing financial interests or personal relationships that could have appeared to influence the work reported in this paper.

Acknowledgments

This work is supported by Beijing Natural Science Foundation (No. 2232062) and the Fundamental Research Funds for the Central Universities (No. 2652022006).

Supplementary materials

Supplementary material associated with this article can be found, in the online version, at doi:10.1016/j.cclet.2024.109771.

References

[1] J. Liang, X.A. Ning, J. Sun, et al., J. Clean. Prod. 204 (2018) 12–19.
[2] K. Ranganathan, K. Karunagaran, D.C. Sharma, Conserv. Recycl. 50 (2007) 306–318.
[3] A.M.S. Jorge, K.K. Athira, M.B. Alves, R.L. Gardas, J.F.B. Pereira, J. Water Process Engin. 55 (2023) 104125.
[4] A. Singh, D.B. Pal, A. Mohammad, et al., Bioresour. Technol. 343 (2022) 126154.
[5] F. Alakhras, E. Alhajri, R. Haounati, et al., Surf. Interf. 20 (2020) 100611.
[6] C.J. Miller, H. Yu, T.D. Waite, Colloid. Surf. A: Physicochem. Engin. Aspects 435 (2013) 147–153.
[7] M.P. Hoyeck, G. Matteo, E.M. MacFarlane, I. Perera, J.E. Bruin, Am. J. Physiol.-Endocrinol.d Metabol. 322 (2022) E383–E413.
[8] C.Y. Zhu, M.T. Shen, M.J. Qi, et al., Dyes Pigments 219 (2023) 111607.
[9] D. Xu, H. Ma, J. Cleaner Prod. 313 (2021) 127758.
[10] N.T. Thao, D.T.H. Ly, H.T.P. Nga, D.M. Hoan, J. Environ. Chem. Engin. 4 (2016) 4012–4020.
[11] M. Saeed, A. Ahmad, et al., Environ. Chem. Lett. 16 (2018) 287–294.
[12] V. Katheresan, J. Kansedo, S.Y. Lau, J. Environ. Chem. Engin. 6 (2018) 4676–4697.
[13] E. Routoula, S.V. Patwardhan, Environ. Sci. Technol. 54 (2020) 647–664.
[14] A.V. Mohod, M. Momotko, N.S. Shah, et al., Water Resour. Ind 30 (2023) 100220.
[15] M. Priyadarshini, I. Das, M.M. Ghangrekar, L. Blaney, J. Environ. Manage. 316 (2022) 115295.
[16] F.C. Moreira, R.A.R. Boaventura, E. Brillas, V.J.P. Vilar, Appl. Catal. B: Environ. 202 (2017) 217–261.
[17] M. Manna, S. Sen, Environ. Sci. Pollut. Res. Int. 30 (2023) 25477–25505.
[18] J.H. Sun, S.H. Shi, Y.F. Lee, S.P. Sun, Chem. Engin. J. 155 (2009) 680–683.
[19] E. Elmolla, M. Chaudhuri, J. Hazard. Mater. 170 (2009) 666–672.
[20] D. Gümüş, F. Akbal, Process Saf. Environ. Protect. 103 (2016) 252–258.
[21] A.K. Al-Buriahi, A.A. Al-Gheethi, P. Senthil Kumar, et al., Chemosphere 287 (2022) 132162.
[22] N. Wang, T. Zheng, G. Zhang, P. Wang, J. Environ. Chem. Engin. 4 (2016) 762–787.
[23] N. Thomas, D.D. Dionysiou, S.C. Pillai, J. Hazard. Mater. 404 (2021) 124082.
[24] Q. Wang, H. Qin, J. Fan, H. Xie, Jo. Hazardous Mater. 443 (2023) 130278.
[25] J. He, X. Yang, B. Men, D. Wang, J. Environ. Sci. 39 (2016) 97–109.
[26] P.V. Nidheesh, RSC Adv. 5 (2015) 40552–40577.
[27] S. Beldjoudi, K. Kouachi, S. Bourouina-Bacha, et al., React. Kinetics Mech. Catal. 133 (2021) 139–155.
[28] B. Jain, A.K. Singh, H. Kim, E. Lichtfouse, V.K. Sharma, Environ. Chem. Lett. 16 (2018) 947–967.
[29] Y. Zhu, Q. Xie, F. Deng, et al., Separation Purif. Technol. 325 (2023) 124702.
[30] S. Lu, L. Liu, H. Demissie, G. An, D. Wang, Environ. Int. 146 (2021) 106273.
[31] Y. Wang, Y. Wang, L. Yu, R. Wang, X. Zhang, Chem. Engin. J. 390 (2020) 124550.
[32] C. Bao, A. Serrano-Lotina, M. Niu, et al., Chem. Engin. J. 466 (2023) 142902.
[33] X.Q. Liu, X.H. Yan, J. Liang, H.X. Kuang, Y.G. Xia, Int. J. Biol. Macromol. 237 (2023) 124107.
[34] Z. Ai, P. Yang, X. Lu, J. Hazard. Mater. 124 (2005) 147–152.
[35] L. Ling, Y. Feng, H. Li, et al., Appl. Surf. Sci. 483 (2019) 772–778.
[36] Y. Gao, Y. Liu, D. Zou, Environ. Chem. Lett. 21 (2023) 2399–2416.
[37] A. de la Hoz, Á. Díaz-Ortiz, A. Moreno, Chem. Soc. Rev. 34 (2005) 164–178.
[38] C. Xue, Y. Mao, W. Wang, et al., J. Environ. Sci. (China) 81 (2019) 119–135.
[39] L. Tian, G. Lv, M. Liu, et al., Progr. Nat. Sci. Mater. Int. 32 (2022) 665–673.
[40] W. Ao, J. Fu, X. Mao, et al., Renew. Sustain. Energy Rev. 92 (2018) 958–979.
[41] S. Głowniak, B. Szczęśniak, J. Choma, M. Jaroniec, Adv. Mater. 33 (2021) 2103477.
[42] M. Green, X. Chen, J. Materiomics 5 (2019) 503–541.

[43] C. Mu, J. Song, B. Wang, et al., J. Alloys Compd. 741 (2018) 814–820.
[44] W. Zheng, W. Ye, P. Yang, et al., Molecules 27 (2022) 4117.
[45] M.M. Butala, M.A. Perez, S. Arnon, et al., Solid State Sci. 74 (2017) 8–12.
[46] W. Gu, G. Lv, L. Liao, et al., J. Hazard. Mater. 338 (2017) 428–436.
[47] L.Y. Novoselova, Appl. Surf. Sci. 539 (2021) 148275.
[48] S. Shimizu, N. Matubayasi, Langmuir 39 (2023) 6113–6125.
[49] Z. Zhang, J. Sun, X. Chen, et al., Appl. Surf. Sci. 622 (2023) 156860.
[50] L. Xu, J. Wang, Appl. Catal. B: Environ. 123-124 (2012) 117–126.
[51] F. Grandjean, G.J. Long, Chem. Mater. 33 (2021) 3878–3904.
[52] X. Chen, K. Zhu, M.A. Ahmed, J. Wang, C. Liang, Chin. J. Catal. 37 (2016) 727–734.
[53] K. Komędera, A. Pierzga, A. Błachowski, et al., J. Alloys Compd. 717 (2017) 350–355.
[54] G.A. Sawatzky, J.M.D. Coey, A.H. Morrish, J. Appl. Phys. 40 (2003) 1402–1403.
[55] M.R. Haider, W.L. Jiang, J.L. Han, et al., Environ. Sci. Technol. 57 (2023) 18668–18679.
[56] M.I. Ahmad, N. Bensalah, Int. J. Environ. Sci. Technol. 19 (2022) 10119–10130.
[57] Z. Wang, H. Zhao, H. Qi, X. Liu, Y. Liu, Environ. Technol. 40 (2019) 1138–1145.
[58] H.A. Martinez-Rodriguez, K. Onyekachi, A. Concha-Balderrama, et al., J. Alloys Compd. 816 (2020) 152668.
[59] C. Xiong, Q. Ren, X. Liu, et al., Appl. Surf. Sci. 543 (2021) 148844.
[60] M. Zhou, H. Yang, T. Xian, et al., J. Hazard. Mater. 289 (2015) 149–157.